JACS JOURNAL OF THE AMERICAN CHEMICAL SOCIETY

Article

Cite This: J. Am. Chem. Soc. 2017, 139, 2345-2350

pubs.acs.org/JACS

Anisotropic Self-Assembly of Supramolecular Polymers and Plasmonic Nanoparticles at the Liquid−Liquid Interface

Joseph J. Armao IV,[†] Irina Nyrkova,[‡] Gad Fuks,[†] Artem Osypenko,[†] Mounir Maaloum,[†] Emilie Moulin,[†] Raul Arenal,[§,⊥] Odile Gavat,[†] Alexander Semenov,*[,‡] and Nicolas Giuseppone*[,†]

[†]SAMS Research Group, Institut Charles Sadron, University of Strasbourg−CNRS, 23 rue du Loess, BP 84047, 67034 Cedex 2 Strasbourg, France

[‡]Institut Charles Sadron−CNRS, 23 rue du Loess, BP 84047, 67034 Cedex 2 Strasbourg, France

[§]Laboratorio de Microscopias Avanzadas (LMA), Instituto de Nanociencia de Aragon (INA), U. Zaragoza, 50018 Zaragoza, Spain

[⊥]Fundacion ARAID, 50018 Zaragoza, Spain

Supporting Information

ABSTRACT: The study of supramolecular polymers in the bulk, in diluted solution, and at the solid−liquid interface has recently become a major topic of interest, going from fundamental aspects to applications in materials science. However, examples of supramolecular polymers at the liquid−liquid interface are mostly unexplored. Here, we describe the supramolecular polymerization of triarylamine molecules and their light-triggered organization at a chloroform−water interface. The resulting interfacial nematic layer of these 1D supramolecular polymers is further used as a template for the precise alignment of spherical gold nanoparticles coming from the water phase. These hybrid thin films are spontaneously formed in a single process, without chemical prefunctionalization of the metallic nanoparticles, and their ordering is improved by centrifugation. The resulting polymer chains and strings of nanoparticles can be co-aligned with high anisotropy over very large distances. By using a combination of experimental and theoretical investigations, we decipher the full sequence of this oriented self-assembly process. In such a highly anisotropic configuration, electron energy loss spectroscopy reveals that the self-assembled nanoparticles behave as plasmonic waveguides.

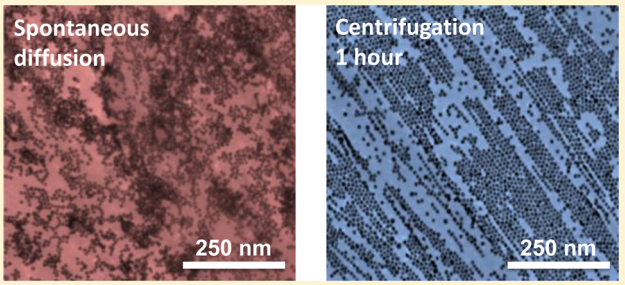

INTRODUCTION

Supramolecular polymers are composed of monomeric units held together by highly directional secondary interactions and with a general behavior following the well-established theories of polymer physics.[1,2] Although high degrees of polymerization can be reached, the kinetic lability between the monomers leads to original dynamic behaviors that are supported by their sensitivity to weak external stimuli[3−5] and by their self-healing properties.[6−8] Supramolecular polymerization is thus of high fundamental interest and results in new materials which have been extensively studied in the bulk and in diluted solutions,[9−11] as well as at the solid−liquid interface.[12−16] However, to the best of our knowledge, supramolecular polymers at the liquid−liquid interface (LLI) have not yet received clear attention in the literature, nor toward fundamental or applied research.[17−19] In this paper, we describe the ordered self-assembly of an interfacial layer of supramolecular polymer chains that takes place at the LLI. To illustrate the potential of such interfacial supramolecular polymers, we show that this layer can serve as a highly anisotropic template to order nanoparticles at the LLI. The method thus appears to be of broad interest to access anisotropic hybrid materials and, for instance, to build soft anisotropic plasmonic substrates.

Indeed, up to now, the strategies studied to access precisely oriented arrangements of plasmonic nanoparticles with emergent collective properties[20−23] can be divided into three categories: (*i*) manipulation methods using top-down technologies;[24−26] (*ii*) templating methods from solution which include the engineering of various organizing substrates such as DNA,[27,28] viruses,[29] and block copolymers;[30,31] and (*iii*) interfacial methods which include liquid−air (Langmuir−Blodgett trough)[32] and liquid−solid interface (patterned surfaces of block copolymers).[33] Further, a particularly appealing technology that can be envisioned to aggregate nanoparticles in films consists of their self-assembly at the liquid−liquid interface.[34−40] LLI platforms are indeed very attractive because they can be formed without the requirement of advanced engineering tools, they are self-healing, and they are easily renewable. Recently, isotropic films of nanoparticles at the LLI have been formed and used as conductive mirror-like coatings[41] and as sensors via in situ surface-enhanced Raman

Received: November 2, 2016
Published: January 18, 2017

DOI: 10.1021/jacs.6b11179
J. Am. Chem. Soc. 2017, 139, 2345−2350

scattering (SERS).[42] However, reaching anisotropic self-assembly of spherical nanoparticles at LLIs is much more challenging, thus precluding their use for a number of optoelectronic plasmonic devices.[43,44] Therefore, the potential use of monodimensional supramolecular polymers at the LLI as anisotropic templating substrates is of particular interest in this direction.

RESULTS AND DISCUSSION

The interfacial films of the present study are formed spontaneously upon shaking using a biphasic system consisting (*i*) of a chloroform phase, at the bottom, containing supramolecular nanofibers based on triarylamine trisamide **1** irradiated for 1 h with white light;[45−53] and (*ii*) of an aqueous phase, at the top, containing a suspension of 12 nm diameter spherical gold nanoparticles (AuNPs) coated with citrate molecules (Figure 1A). Imaging of the film by atomic force microscopy (AFM) in Figure 1B revealed two distinct sides comprising (*i*) one layer of triarylamine fibrils at the bottom, and (*ii*) one layer of AuNPs at the top.

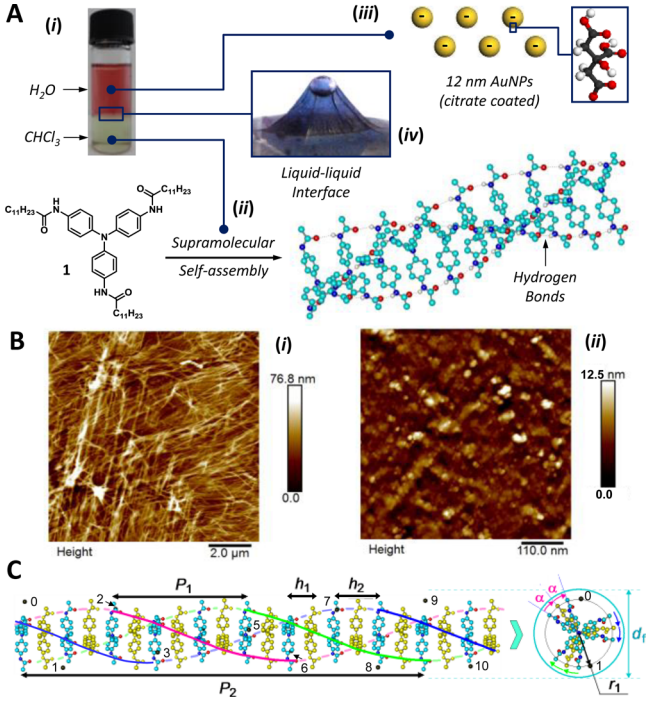

Figure 1. (A) (*i*) Photograph of the biphasic (chloroform/water) system; (*ii*) chloroform solution contains triarylamine **1**, which is self-assembled in helical fibrils that are doped by partial photo-oxidation of **1** to $\mathbf{1}^{\bullet+}$; (*iii*) water phase contains a suspension of gold nanoparticles (AuNPs) being coated by negatively charged citrate molecules; (*iv*) hybrid film formed at the LLI, which is here photographed with an air bubble trapped inside. (B) AFM height images of the film from the bottom side (*i*) and from the top side (*ii*). (C) Helical structure of a supramolecular fibril containing 50% of neutral units **1** (shown in yellow), 50% of charged units $\mathbf{1}^{\bullet+}$, and surrounded by the chloride counterions (black balls numbered from 0 to 10).[54] The colored lines indicate the three "chains" of amide groups connected by hydrogen bonds; three characteristic periods within the fibril (h_1, P_1, P_2): $h_2 = 2h_1 = 0.970$ nm, contour length per radical; $d_f = 1.7$ nm, effective fibril thickness; $r_1 = 0.7$ nm, radial displacement of condensed chloride ions from the fibril axis (distance between Cl^- and the central N^+ of $\mathbf{1}^{\bullet+}$ radical). In the helical stack, each molecule is rotated by the angle $\alpha = 360°/18 = 20°$ with respect to the previous one.

Importantly, the preirradiation of the chloroform solution of triarylamines with a halogen lamp (leading to the partial photo-oxidation of the fibers in the form of $\mathbf{1}^{\bullet+}$)[47] is mandatory for the film formation. Indeed, control experiments performed in the dark did not produce any film at any concentration. In addition, the presence of the triarylamines is necessary to accumulate the nanoparticles at the LLI. Indeed, a control experiment in the presence of light and only AuNPs revealed their stable suspension in water for weeks (see Supporting Information section 3a). Finally, negatively charged AuNPs are necessary to produce a hybrid layer. Indeed, by using cationic nanoparticles coated with ammonium and obtained by ligand exchange from the citrated ones (see Supporting Information section 3b), no hybrid film was formed using the same experimental protocol.

Visible absorption measurements display a 90 nm red shift between the colloidal nanoparticle suspension and the interfacial film (Figure 2A), which is a typical plasmonic effect for nanoparticles being in close contact. Examination of the interfacial film with a confocal Raman microscope also revealed a SERS effect indicating the close proximity of the triarylamine nanofibers with the AuNPs (Figure 2B, blue). All of the peaks observed are due to the vibronic signature of the polymer which is enhanced by the SERS effect. This signal is only observed when focusing the laser on areas with triarylamine nanofibers and AuNPs, whereas no signal is observed when focusing the laser on areas with solely nanofibers (Figure 2B, black). Remarkably, when the agitation method was changed from shaking to stirring, we observed a partial anisotropic ordering of the AuNPs and nanofibers in some locations of the film. We hypothesized that the lateral force being applied to the film interface during the stirring was responsible for this partial organization. In order to make the results more regular, we performed a series of experiments using a swinging bucket centrifuge with a controlled rotation speed. Transmission electron microscopy (TEM) images of the hybrid films were obtained for different centrifugal forces (*g*), starting from a 5 mM chloroform solution of **1** and a 1.3×10^{-9} M suspension of AuNPs (Figure 2C). This series of micrographs reveals a marked improvement of the nanoparticle alignment upon centrifugation, reaching almost perfect orientations over large domains for the higher rotation speeds. This long-range ordering was further evidenced at higher scale by cross-polarized optical microscopy, showing the formation of a nematic liquid-crystal phase with large domain sizes when increasing the centrifugation rate (Figure 2D). Similar ordering was also measured with larger AuNPs having a diameter of 44 nm (see Supporting Information section 3c and Figure S12). To the best of our knowledge, no comparable ordering of nanoparticles at the LLI and on such large scale has been reported in the literature.

Quantification of the anisotropy for different centrifugal forces was determined by a statistical analysis of a series of TEM images over three characteristic surface areas between 2.25 and 25 μm^2 (Figure 3) and quantified using the orientational parameter *S* ($0 \leq S \leq 1$). For concentration $c = 5$ mM of **1**, and for all the surface areas considered, *S* was improved with the rotation speed. For instance, it was possible to reach $S = 0.76$ at 10*g* for a surface of 25 μm^2 (Figure 3A(*iii*)), with $S = 0.18$ at 0*g* for the same surface (Figure 3A(*i*)). Interestingly, the quality of the ordering was further improved by working at a lower concentration of **1** ($c = 1$ mM). Considering again the larger surface area (25 μm^2), *S* is

DOI: 10.1021/jacs.6b11179
J. Am. Chem. Soc. 2017, 139, 2345−2350

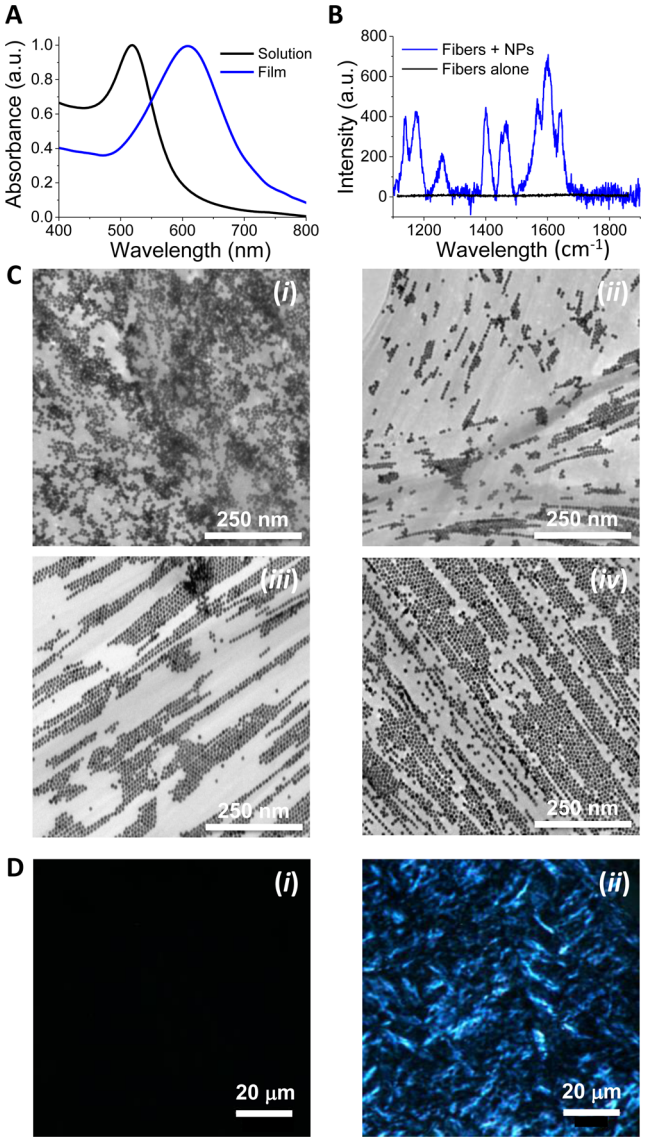

Figure 2. (A) Extinction spectra of the plasmonic film of AuNPs compared to their colloidal suspension. (B) SERS response of the hybrid film containing fibers and nanoparticles (blue) and of regions containing only fibers (black). (C) Typical TEM images of the film formed at the LLI (c(**1**) = 5 mM) for the following centrifugation conditions: (*i*) 0*g* and overnight free diffusion, (*ii*) 5*g* for 1 h, (*iii*) 100*g* for 1 h, (*iv*) 1000*g* for 1 h. (D) Optical microscopy under crossed polarizers for the following centrifugation conditions: (*i*) 0*g* and overnight free diffusion, (ii) 1000*g* for 1 h.

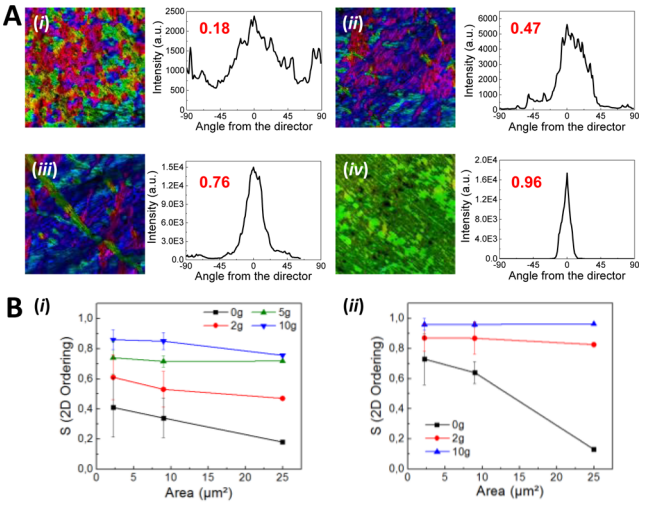

Figure 3. (A) TEM images (squares with the surface = 5 μm × 5 μm) were analyzed to determine the angular space correlation alignment intensity distributions (plots) and the resulting orientational parameter S (value given in red); each color reflects a particular orientation of the nanoparticle strings; (*i*) no centrifugation, overnight diffusion starting with a 5 mM solution of **1**; (*ii*) 1 h centrifugation of 2*g* starting with a 5 mM solution of **1**; (*iii*) 1 h centrifugation of 10*g* starting with a 5 mM solution of **1**; (*iv*) 1 h centrifugation of 10*g* starting with a 1 mM solution of **1**. (B) Orientational parameter S as a function of the surface area and of the applied centrifugal force starting from a 5 mM solution of **1** (*i*) and a 1 mM solution of **1** (*ii*). Error bars are established for over 16 measurements for each centrifugal force.

increased from 0.13 at 0*g* (no ordering) to 0.96 at 10*g* (almost perfect ordering) (Figure 3A(*iv*)). At the same concentration (c(**1**) = 1 mM), one can also notice that, for smaller surface areas, a partial anisotropic ordering is observed even without centrifugation (S = 0.62 for 9 μm^2 and S = 0.73 for 2.25 μm^2) (Figure 3B(*ii*)).

The mechanism for the highly anisotropic co-self-assembly that occurs at the LLI is first related to the structure and dynamics of the supramolecular polymers in the organic phase. As shown in Figure 1C, molecule **1** self-assembles in single-columnar aggregates (fibrils) with a helical stacking structure[47] having three characteristic periods: $h_1 \approx 0.485$ nm (contour length per molecule), $P_1 = 6h_1$ (apparent helical period), and $P_2 = 3P_1$ (full helical pitch). Upon 1 h of light irradiation, the fibrils become charged with ~50% of units in the radical cation state (**1**$^{\bullet+}$ with central N$^+$). Due to the low dielectric constant of chloroform, the Cl$^-$ counterions (coming from the reduction of chloroform) are condensed onto the fibrils and are themselves arranged helically around the fibril with a pitch of P_2 (see black balls in Figure 1C and Figure S2). The fibrils are stabilized by three hydrogen bonds per molecule, aromatic $\pi-\pi$ stacking, and Coulomb (dipole−dipole) interactions. The fibril scission energy $E_{sc} \sim 24.5k_BT$ (estimated by all-atomic modeling including solvation effects)[48] is high enough to ensure very low critical aggregation concentration. The length distribution of fibrils is defined by the balance between fibril scission and fusion events (the end evaporation mechanism[55] is subdominant for long fibrils): $(n) + (m) \rightleftharpoons (n + m)$, that is, $c_{n+m} = Kc_nc_m$, where c_n is concentration of n-mers. The scission probability is defined by E_{sc}, whereas fusion is associated with entropy loss (confinement to the effective bond volume, v_b), leading to an equilibrium constant of the reaction $K = v_b e^{E_{sc}/k_BT}$. Remarkably, the fusion is accelerated in the presence of photoinduced radicals because fibril ends are then decorated with N$^+$Cl$^-$ dipoles attracting each other (with an energy E_{dd}) and thus increasing the frequency of end collisions (Figure S3). As a result, the fusion constant increases significantly (by ~10^4): $K \rightarrow K^* = Ke^{E_{dd}/k_BT}$. The scission/fusion process is not affected otherwise as the end dipoles annihilate on contact by the following binary reduction reaction: $2(N^+ + Cl^-) \rightarrow 2N + Cl_2$ (Figure S2C).[48] Accordingly, the mean fibril length of linear fibrils $\bar{L} \simeq h_1(K^*c)^{1/2}$ strongly increases (see supplementary equation S1). Based on the experimental $\bar{L} \sim 1$ μm at c = 1 mM (Figure S4D), we get $E_{sc} \approx 24.7k_BT$, in agreement with E_{sc} obtained by modeling. The fibril persistence length $l_p \approx 20$ nm is obtained (see supplementary equation S2) based on the mean contour length of supertwisted rings $\bar{L}_{ring} \sim 250$ nm at c =

DOI: 10.1021/jacs.6b11179
J. Am. Chem. Soc. 2017, 139, 2345−2350

0.1 mM (Figure S4A–C). In a hierarchical organization process, two fibrils then attract each other side-to-side mainly due to Coulomb interactions of ionized $\mathbf{1}^{\bullet+}$ and Cl^- counterions. The attraction is stronger for fibrils of opposite chiralities (see Supporting Information section 2a), but in all cases, it is not enough to overcome entropic penalty for double columnar complex formation. Bundles of many fibrils may be, however, stable due to their higher rigidity, but their nucleation requires higher concentration, $c \gtrsim 5$ mM, as verified experimentally by AFM imaging (Figure S4E).

In the biphasic chloroform/water systems, the fibrils are mostly hydrophobic and remain in the organic phase. However, the Cl^- counterions strongly prefer water phase to bulk chloroform in spite of their electrostatic binding on triarylamine fibrils (see Supporting Information section 2b and Figure S5). As a result, some Cl^- ions escape from fibrils located near the interface and leave them charged. The charged fibrils are thus driven to the interface by interactions with the opposite image charges (due to high dielectric constant of water). This trend was supported experimentally by measuring the interfacial tension between chloroform and water: it is shown to drop from 32.5 $mN{\cdot}m^{-1}$ for a nonirradiated chloroform solution of **1** (c = 1 mM) to 26 $mN{\cdot}m^{-1}$ after irradiation of 1 h, confirming the migration of the charged fibers towards the LLI (see Supporting Information sections 2b and 3d and Figure S13). The total energy gain on fibril adsorption is $\Delta F \approx -5k_BT$ per contour length segment, $\Delta L = h_2 \approx 1$ nm for optimal fraction $f_t \approx 1/3$ of transferred counterions (Figure S5). Being strongly attracted electrostatically to the LLI, the fibrils tend to form there a dense adsorbed monolayer and thus to order. Indeed, at thermodynamic equilibrium, because of geometrical constraints and because of their side-to-side electrostatic attraction, the fibrils must be aligned nearly parallel with a high nematic order (i.e., with orientational parameter S close to 1). In practice, however, and in contrast to their fast diffusion-controlled adsorption taking ~1 s for c = 1 mM, the ordering process is very slow. This is due to the slow dynamics of long ($\overline{L} > 1$ μm; $M_w > 1.6 \times 10^6$ g mol^{-1}) and rigid fibrils in dense confined conditions at the surface[56] involving jamming and long-lasting defects like fibril crossings (Figure S6). Vibrations during the centrifugation process may induce interfacial waves aiding to heal the orientational defects and providing longer-range fibril alignment (see Supporting Information section 2b for a detailed explanation). In addition, the charged monolayer of fibrils induces positive potential $\zeta_i = 1.45k_BT/e$ in water close to the interface with chloroform. The fibril charge is compensated by condensed and diffused layers of anions (mostly citrate trianions) in water close to the LLI (Figure S7).

Turning to AuNPs in the aqueous phase, we established that they are protected by adsorbed layers of condensed hydrated ions: alternating Na^+ cations and citrate anions adsorbed directly on the gold surface (see Supporting Information section 2c). The ion layer shows a total thickness $h_{st} \approx 1.5$ nm (Figure S8) and is indispensable for steric stabilization of AuNPs at short distances. At larger separations, the nanoparticles are stabilized electrostatically due to their negative surface ζ-potential, $\zeta_s = -1.9k_BT/e$. The AuNPs are thus attracted by the oppositely charged interface containing the supramolecular fibrils. As they approach it closer than ~5 nm, the condensed interfacial anions are driven away by their repulsion with AuNPs, thus increasing the effective positive interfacial charge by a factor of 5 (see Supporting Information section 2c). The resultant attraction energy amounts to ~$110k_BT$, ensuring strong adsorption of AuNPs on the LLI. It is remarkable that even uncharged AuNPs would be adsorbed on the interface with charged supramolecular fibrils as the net attraction energy of ~$10k_BT$ is due to induction of a negative charge in the AuNP surface region opposite to the interface. The kinetics of irreversible adsorption of AuNPs on the interface is controlled by their diffusion/sedimentation aided by centrifugation. The NPs then tend to form a well-organized hexagonal structure at the interface as soon as a significant surface coverage is achieved. Remarkably, for less dense regions, micrographs mostly show ordered elongated clusters following orientation of the aligned fibrils because the adsorbed NPs attract each other laterally due to a significant redistribution of their surface charge caused by the proximity of positively charged fibrils (Figure S9).

To probe further the optical properties of the hybrid film, we performed high-resolution electron energy loss spectroscopy (HR-EELS)[57,58] measurements to study the local plasmonic response of aligned AuNPs obtained at 10 g and $c(\mathbf{1})$ = 5 mM (Figure 4). An EELS spectrum-image (SPIM) in the low-loss region (below 50 eV) is shown in Figure 4C for two NPs in close contact (and obtained from the green marked area of Figure 4A). The intensity maps of the local surface plasmon resonances (LSPRs) extracted from this EELS-SPIM show blue shifts and broadenings of the dipolar LSPR mode at ~2.2 eV, typical for two spherical NPs arranged in a more ellipsoidal shape (Figure 4C,D).[47] The behavior of these LSPR modes strongly depends on the dielectric environment of the NPs (Figure 4D(ii)).[56,59] A shift and an extra contribution at higher energy (above 2.4 eV) can be observed in this EEL spectrum,

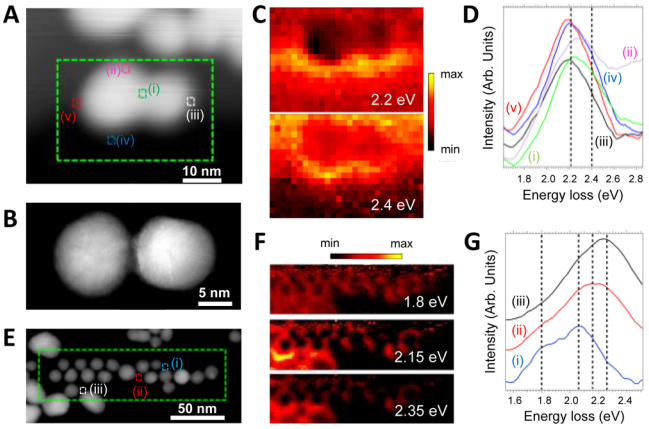

Figure 4. (A) Low-magnification high-angle annular dark-field (HAADF) scanning transmission electron microscopy (STEM) image of two Au nanoparticles at close distance. (B) High-resolution HAADF-STEM image of two other Au nanoparticles, showing their high crystalline quality degree. (C) Intensity maps extracted from the EELS-SPIM recorded in the green marked area of (A), after removing the zero-loss peak (ZLP). These intensity maps show the spatial distribution of the LSPR mode of these AuNPs. (D) EEL spectra (each of them corresponds to the sum of four spectra) extracted from the EELS-SPIM in the areas marked in (A) and labeled as (i–v), respectively. (E) Low-magnification HAADF-STEM image of a typical string of spherical AuNPs. An EELS-SPIM has been recorded in the squared area marked in green. (F) Intensity maps extracted from the EELS-SPIM after removing the ZLP and showing the spatial distribution of the LSPR modes. (G) EEL spectra (each of them corresponds to the sum of four spectra) obtained from the EELS-SPIM in the regions marked in (E).

DOI: 10.1021/jacs.6b11179
J. Am. Chem. Soc. 2017, 139, 2345–2350

which can be due to the substrate effect or the presence of the NPs at the top.[59] A HAADF-STEM image of a longer string of Au nanoparticles is shown in Figure 4E. The intensity maps extracted from the low-loss EELS-SPIM acquired on the green marked area show the spatial distribution of the excited LSPR modes, corresponding to the plasmon resonances couplings of the different NPs (Figure 4F). The peaks observed in Figure 4G correspond to LSPR (different (dark and bright) transversal/longitudinal) modes shown in the intensity maps.[60]

The enhancement of the electromagnetic field is maximal in the hot spots (gap between the NPs) as it is expected for surface plasmon couplings in linear chains of NPs.[60] This demonstrates that this self-assembly method induces plasmonic waveguide behavior due to ordering of the hybrid film.

CONCLUSION

To summarize, the basic features of the co-self-assembly at LLI described here involve (*i*) a light-assisted supramolecular polymerization of neutral and oxidized cationic triarylamine units producing long positively charged hydrophobic filaments whose length and periodic structure are greatly enhanced by photodoping;[47] (*ii*) a transfer of counterions to the favorable aqueous environment rendering the filaments positively charged and trapped near the interface by attraction to the image charge; (*iii*) a further growth and a nematic packing by dynamic scission/recombination of the supramolecular polymer fibers at the LLI; (*iv*) an adsorption of negatively charged AuNPs dispersed in water on the LLI. The resultant interfacial structure comprises a highly anisotropic layer of conductive supramolecular fibrils and a plasmonic layer of AuNPs. The nematic self-assembled structure of AuNPs reflects the order of the underlying fibril layer. Overall, the light-controlled supramolecular organization at the LLI, the use of supramolecular polymers as nematic templates, the hybrid inorganic−organic nature of the film, the superior level of anisotropy that can be reached compared to the present literature, and the verified plasmonic coupling between the AuNPs are of particular fundamental interest and opens interesting perspectives for potential applications of such anisotropic functional structures in material science. Although we have shown that such a self-assembled system requires particular constraints to function properly, it is unlikely that it would represent a unique example. Our theoretical analysis invites us to further probe experimentally its generality and robustness. It stimulates a search for new systems where Coulomb forces can drive complex nanostructure formation at the LLI. The scope of this self-assembly process will be the subject of our future research by using for example (*i*) other organic molecules capable of 1D self-assembly and including ionic groups, (*ii*) covalent polymeric ionomer in an organic medium, (*iii*) other metal nanoparticles dispersed in water, either charged or even uncharged.

ASSOCIATED CONTENT

Supporting Information

The Supporting Information is available free of charge on the ACS Publications website at DOI: 10.1021/jacs.6b11179.

Experimental protocols, additional theoretical aspects of supramolecular fibrils and AuNP organization, and control experiments (PDF)

AUTHOR INFORMATION

Corresponding Authors

*alexander.semenov@ics-cnrs.unistra.fr

*giuseppone@unistra.fr

ORCID

Raul Arenal: 0000-0002-2071-9093

Nicolas Giuseppone: 0000-0003-4093-3000

Notes

The authors declare no competing financial interest.

ACKNOWLEDGMENTS

The research leading to these results has received funding from the European Research Council/ERC Starting Grant Agreement No. 257099 (N.G.). We thank the IRTG for a postdoctoral fellowship to I.N. We also thank the LabEx CSC and the icFRC of Strasbourg. We acknowledge the Electron Microscopy Facility of the Institut Charles Sadron. The HRSTEM and EELS measurements were performed in the Laboratorio de Microscopias Avanzadas (LMA) at the Instituto de Nanociencia de Aragon (INA), Universidad de Zaragoza (Spain). Some of the research leading to these results has received funding from the European Union Seventh Framework Programme under Grant Agreement 312483-ESTEEM2 (Integrated Infrastructure Initiative − I3). R.A. gratefully acknowledges the support from the Spanish Ministerio de Economia y Competitividad (FIS2013-46159-C3-3-P and MAT2016-79776-P) and from the European Union H2020 program ETN project "Enabling Excellence" Grant Agreement 642742. We thank Dr. Matthias Pauly, Dr. Wiebke Drenckhan, Dr. François Schosseler, and Mélodie Galerne for help at various stages.

REFERENCES

(1) Brunsveld, L.; Folmer, B. J. B.; Meijer, E. W.; Sijbesma, R. P. *Chem. Rev.* **2001**, *101*, 4071.

(2) Ciferri, A. *Supramolecular Polymers*, 2nd ed.; Ciferri, A., Ed.; CRC Press: Boca Raton, FL, 2005.

(3) Yan, X.; Wang, F.; Zheng, B.; Huang, F. *Chem. Soc. Rev.* **2012**, *41*, 6042.

(4) Ma, X.; Tian, H. *Acc. Chem. Res.* **2014**, *47*, 1971.

(5) Jones, C. D.; Steed, J. W. *Chem. Soc. Rev.* **2016**, *45*, 6546−6596.

(6) Yang, Y.; Urban, M. W. *Chem. Soc. Rev.* **2013**, *42*, 7446.

(7) Herbst, F.; Döhler, D.; Michael, P.; Binder, W. H. *Macromol. Rapid Commun.* **2013**, *34*, 203.

(8) van Gemert, G. M. L.; Peeters, J. W.; Söntjens, S. H. M.; Janssen, H. M.; Bosman, A. W. *Macromol. Chem. Phys.* **2012**, *213*, 234.

(9) De Greef, T. F. A.; Smulders, M. M. J.; Wolffs, M.; Schenning, A. P. H. J.; Sijbesma, R. P.; Meijer, E. W. *Chem. Rev.* **2009**, *109*, 5687.

(10) Aida, T.; Meijer, E. W.; Stupp, S. I. *Science* **2012**, *335*, 813.

(11) Busseron, E.; Ruff, Y.; Moulin, E.; Giuseppone, N. *Nanoscale* **2013**, *5*, 7098.

(12) De Feyter, S.; De Schryver, F. C. *Chem. Soc. Rev.* **2003**, *32*, 139.

(13) Ciesielski, A.; Palma, C.-A.; Bonini, M.; Samorì, P. *Adv. Mater.* **2010**, *22*, 3506.

(14) van Hameren, R.; van Buul, A. M.; Castriciano, M. A.; Villari, V.; Micali, N.; Schön, P.; Speller, S.; Monsù Scolaro, L.; Rowan, A. E.; Elemans, J. A. A. W.; Nolte, R. J. M. *Nano Lett.* **2008**, *8*, 253.

(15) Yang, H.; Ma, Z.; Yuan, B.; Wang, Z.; Zhang, X. *Chem. Commun.* **2014**, *50*, 11173.

(16) Sakai, N.; Bhosale, R.; Emery, D.; Mareda, J.; Matile, S. *J. Am. Chem. Soc.* **2010**, *132*, 6923.

(17) We here consider the restriction of supramolecular polymers as defined in ref 1. For examples of self-assemblies at the liquid−liquid interface of nanostructures other than supramolecular polymers, see refs 18 and 19.

DOI: 10.1021/jacs.6b11179
J. Am. Chem. Soc. 2017, 139, 2345−2350

(18) Niu, Z.; He, J.; Russell, T. P.; Wang, Q. *Angew. Chem., Int. Ed.* **2010**, *49*, 10052.
(19) Hu, L.; Chen, M.; Fang, X.; Wu, L. *Chem. Soc. Rev.* **2012**, *41*, 1350.
(20) Ozbay, E. *Science* **2006**, *311*, 189.
(21) Nie, Z.; Petukhova, A.; Kumacheva, E. *Nat. Nanotechnol.* **2010**, *5*, 15.
(22) Atwater, H. A.; Polman, A. *Nat. Mater.* **2010**, *9*, 205.
(23) Hentschel, M.; Saliba, M.; Vogelgesang, R.; Giessen, H.; Alivisatos, A. P.; Liu, N. *Nano Lett.* **2010**, *10*, 2721.
(24) Maier, S. A.; Kik, P. G.; Atwater, H. A.; Meltzer, S.; Harel, E.; Koel, B. E.; Requicha, A. A. G. *Nat. Mater.* **2003**, *2*, 229.
(25) Bek, A.; Jansen, R.; Ringler, M.; Mayilo, S.; Klar, T. A.; Feldmann, J. *Nano Lett.* **2008**, *8*, 485.
(26) Maragò, O. M.; Jones, P. H.; Gucciardi, P. G.; Volpe, G.; Ferrari, A. C. *Nat. Nanotechnol.* **2013**, *8*, 807.
(27) Tan, S. J.; Campolongo, M. J.; Luo, D.; Cheng, W. *Nat. Nanotechnol.* **2011**, *6*, 268.
(28) Ross, M. B.; Ku, J. C.; Vaccarezza, V. M.; Schatz, G. C.; Mirkin, C. A. *Nat. Nanotechnol.* **2015**, *10*, 453.
(29) Dujardin, E.; Peet, C.; Stubbs, G.; Culver, J. N.; Mann, S. *Nano Lett.* **2003**, *3*, 413.
(30) Wang, H.; Lin, W.; Fritz, K. P.; Scholes, G. D.; Winnik, M. A.; Manners, I. *J. Am. Chem. Soc.* **2007**, *129*, 12924.
(31) Akcora, P.; Liu, H.; Kumar, S. K.; Moll, J.; Li, Y.; Benicewicz, B. C.; Schadler, L. S.; Acehan, D.; Panagiotopoulos, A. Z.; Pryamitsyn, V.; Ganesan, V.; Ilavsky, J.; Thiyagarajan, P.; Colby, R. H.; Douglas, J. F. *Nat. Mater.* **2009**, *8*, 354.
(32) Huang, J.; Kim, F.; Tao, A. R.; Connor, S.; Yang, P. *Nat. Mater.* **2005**, *4*, 896.
(33) Mistark, P. A.; Park, S.; Yalcin, S. E.; Lee, D. H.; Yavuzcetin, O.; Tuominen, M. T.; Russell, T. P.; Achermann, M. *ACS Nano* **2009**, *3*, 3987.
(34) Toor, A.; Feng, T.; Russell, T. P. *Eur. Phys. J. E: Soft Matter Biol. Phys.* **2016**, *39*, 57.
(35) Aveyard, R.; Binks, B. P.; Clint, J. H. *Adv. Colloid Interface Sci.* **2003**, *100−102*, 503.
(36) Binder, W. H. *Angew. Chem., Int. Ed.* **2005**, *44*, 5172.
(37) Lin, Y.; Skaff, H.; Emrick, T.; Dinsmore, A. D.; Russell, T. P. *Science* **2003**, *299*, 226.
(38) Reincke, F.; Hickey, S. G.; Kegel, W. K.; Vanmaekelbergh, D. *Angew. Chem., Int. Ed.* **2004**, *43*, 458.
(39) Duan, H.; Wang, D.; Kurth, D. G.; Möhwald, H. *Angew. Chem., Int. Ed.* **2004**, *43*, 5639.
(40) Zhang, S.-Y.; Liu, J.-W.; Zhang, C.-L.; Yu, S.-H. *Nanoscale* **2013**, *5*, 4223.
(41) Fang, P.-P.; Chen, S.; Deng, H.; Scanlon, M. D.; Gumy, F.; Lee, H. J.; Momotenko, D.; Amstutz, V.; Cortés-Salazar, F.; Pereira, C. M.; Yang, Z.; Girault, H. H. *ACS Nano* **2013**, *7*, 9241.
(42) Cecchini, M. P.; Turek, V. A.; Paget, J.; Kornyshev, A. A.; Edel, J. B. *Nat. Mater.* **2013**, *12*, 165.
(43) Thorkelsson, K.; Bai, P.; Xu, T. *Nano Today* **2015**, *10*, 48.
(44) Anker, J. N.; Hall, W. P.; Lyandres, O.; Shah, N. C.; Zhao, J.; Van Duyne, R. P. *Nat. Mater.* **2008**, *7*, 442.
(45) Moulin, E.; Niess, F. F.; Maaloum, M.; Buhler, E.; Nyrkova, I.; Giuseppone, N. *Angew. Chem., Int. Ed.* **2010**, *49*, 6974.
(46) Faramarzi, V.; Niess, F.; Moulin, E.; Maaloum, M.; Dayen, J.-F.; Beaufrand, J.-B.; Zanettini, S.; Doudin, B.; Giuseppone, N. *Nat. Chem.* **2012**, *4*, 485.
(47) Armao, J. J.; Maaloum, M.; Ellis, T.; Fuks, G.; Rawiso, M.; Moulin, E.; Giuseppone, N. *J. Am. Chem. Soc.* **2014**, *136*, 11382.
(48) Nyrkova, I.; Moulin, E.; Armao, J. J.; Maaloum, M.; Heinrich, B.; Rawiso, M.; Niess, F.; Cid, J.-J.; Jouault, N.; Buhler, E.; Semenov, A. N.; Giuseppone, N. *ACS Nano* **2014**, *8*, 10111.
(49) Armao, J. J.; Domoto, Y.; Umehara, T.; Maaloum, M.; Contal, C.; Fuks, G.; Moulin, E.; Decher, G.; Javahiraly, N.; Giuseppone, N. *ACS Nano* **2016**, *10*, 2082.
(50) Armao, J. J.; Rabu, P.; Moulin, E.; Giuseppone, N. *Nano Lett.* **2016**, *16*, 2800.
(51) Kim, T.; Mori, T.; Aida, T.; Miyajima, D. *Chem. Sci.* **2016**, *7*, 6689−6694.
(52) Haedler, A. T.; Meskers, S. C. J.; Zha, R. H.; Kivala, M.; Schmidt, H.-W.; Meijer, E. W. *J. Am. Chem. Soc.* **2016**, *138*, 10539.
(53) Kim, J.; Lee, J.; Kim, W. Y.; Kim, H.; Lee, S.; Lee, H. C.; Lee, Y. S.; Seo, M.; Kim, S. Y. *Nat. Commun.* **2015**, *6*, 6959.
(54) Note that ∼50% was the maximum radical content observed in the triarylamine fibrils after 1 h irradiation of a freshly prepared solution of **1** in chloroform.
(55) Semenov, A. N.; Nyrkova, I. A. *J. Chem. Phys.* **2011**, *134*, 114902.
(56) Jordens, S.; Isa, L.; Usov, I.; Mezzenga, R. *Nat. Commun.* **2013**, *4*, 1917.
(57) Nelayah, J.; Kociak, M.; Stéphan, O.; García de Abajo, F. J.; Tencé, M.; Henrard, L.; Taverna, D.; Pastoriza-Santos, I.; Liz-Marzán, L. M.; Colliex, C. *Nat. Phys.* **2007**, *3*, 348.
(58) Prieto, M.; Arenal, R.; Henrard, L.; Gomez, L.; Sebastian, V.; Arruebo, M. *J. Phys. Chem. C* **2014**, *118*, 28804.
(59) Arenal, R.; Henrard, L.; Roiban, L.; Ersen, O.; Burgin, J.; Treguer-Delapierre, M. *J. Phys. Chem. C* **2014**, *118*, 25643.
(60) Barrow, S. J.; Rossouw, D.; Funston, A. M.; Botton, G. A.; Mulvaney, P. *Nano Lett.* **2014**, *14*, 3799.

DOI: 10.1021/jacs.6b11179
J. Am. Chem. Soc. 2017, 139, 2345−2350